TAMPEREEN TEKNILLINEN YLIOPISTO
TAMPERE UNIVERSITY OF TECHNOLOGY

AZIN AKBARI

ADIABATIC SHEAR BANDING IN TITANIUM 15-3-3-3 ALLOY

Master of Science Thesis

Examiners: Professor Veli-Tapani Kuokkala,
Dr. Mikko Hokka,
Examiner and topic approved by the council meeting of the Faculty of Engineering Sciences on 6th March 2013

Abstract:

TAMPERE UNIVERSITY OF TECHNOLOGY

Master's Degree Program in Materials Science

Major: Materials Research

AKBARI, AZIN: Adiabatic Shear Bands in Ti 15-3-3-3 Alloy

Master of Science Thesis, 60 pages

August 2013

Examiners: Professor Veli-Tapani Kuokkala and Dr. Mikko Hokka

Keywords: Split Hopkinson Pressure Bar, Titanium 15-3, Shear bands

Shear stresses are a common reason for failure in many industrial applications. Localized shear deformations in certain materials can lead to the formation of adiabatic shear bands. Titanium alloys in particular have proven to be good candidates for the formation of the adiabatic shear bands. For this reason, this study focuses on the shear behavior of Ti 15-3-3-3 alloy, and especially the shear localizations during deformation at various strain rates. Shear strains are localized into a narrow region in the hat-shaped specimens due to the geometry of the specimen. Therefore, in this study, the mechanical behavior of Ti-15-3-3-3 alloy was studied using the Split Hopkinson Pressure Bar (at high strain rates) and servo-hydraulic materials testing machine (at lower strain rates) using the hat-shape specimens. Stopper rings were used to limit the amount of deformation and consequently the amount of applied strain to a predetermined value. The microstructures of the adiabatic shear bands were studied using optical and scanning electron microscopy. The

widths of the shear bands were measured from the micrographs of the samples with different amounts of deformation. In some samples, also individual slip bands appeared clearly outside the primary shear zone. These individual slip bands were neglected in the calculations of stress vs. strain curves, and therefore the deformation was assumed to be limited to the primary shear band area only. Finally it was concluded that the shear band width is independent of the amount of strain in the high strain rate tests. This constant value was used in the calculations of shear strain and strain rate. The shear stress and shear strain for each test were calculated and the obtained stress-strain curves were analyzed. Different mechanical behavior was observed in the high strain rate test results compared to the results obtained at low strain rates. At high strain rates the effect of strain hardening is significantly weaker than the thermal softening in the primary shear band, leading to a strongly localized deformation and constant shear band width.

Acknowledgements

I would like to express my gratitude to Prof. Veli-Tapani Kuokkala who gave me the chance of working in this friendly environment. Dr. Mikko Hokka is also gratefully acknowledged for the guidance and help throughout this thesis work.

My gratitude also goes to M.Sc. Juha Nykänen, M.Sc. Kauko Östaman, Juuso Perolainen and all other members of the Materials Characterization research group for their help and advice.

I would as well thank my friends Saeed Afrasiabi, Shakiba Fallahi, and Mitra Akbari for their love and support.

Finally, this thesis is dedicated to my family, Mohammad-Ali Akbari, Sima Gholami, and Erfan Akbari, without who my life would have been meaningless.

Tampere, Finland

August 2013.

Azin Akbari

List of Symbols and Abbreviations

A	Shear area of the specimen
A_{bar}	Cross-sectional area of the pressure bars
C	Sound speed in bars
c	Special heat capacity
d	Shear band width
D	Diameter of the specimen
E_{bar}	Young's modulus of the bar material
El	Elongation
F	Load
k	Boltzman's constant
L	Length of the shear zone
M	Orientation factor
P_B	Boltzman's probability
T	Temperature
T_c	Critical temperature
t_w	Waiting time for a dislocation

V_T	Wave speed in the transmitted bar
V_I	Wave speed in the incident bar
Y_s	Tensile Strength
ΔG	Gibbs free energy
Δl	Displacement
ε	Strain
ε_i	Incident axial strain
ε_r	Reflected axial strain
ε_t	Transmitted axial strain
ρ	Density
σ	Flow stress
σ_G	Athermal component of stress
σ^*	Thermal component of stress
T	Shear stress
γ	Shear strain
β	Fraction of mechanical energy converted to heat
υ_0	Vibration frequency of a dislocation

ASB Adiabatic Shear Bands

ASM American Society for Metals

ASTM American Society for Testing and Materials

EDS Energy-dispersive X-ray Spectroscopy

OM Optical Microscopy

RPM Revolutions per Minute

SHPB Split Hopkinson Pressure Bars

SEM Scanning Electron Microscopy

SE Secondary Electrons

UTS Ultimate Tensile Strength

VAR Vacuum Arc Re-melting

Contents

1. Introduction

Materials go through shear deformation in many industrial applications. In many cases the shear deformation occurs at a high rate (e.g. in high speed shaping and forming, machining, and grinding). [1] This high strain rate shear may lead to failure of the material; therefore it is necessary to study the mechanical behavior of the materials during high strain rate shear as well as other forms of deformation.

High strain rate shear might result in a formation of adiabatic shear bands, which can lead to failure. Generally, titanium alloys have low density and low heat conductivity. This makes them very sensitive to the formation of the adiabatic shear bands. [2] Therefore, in this study the mechanical behavior of Titanium 15-3-3-3 (or Ti 15-3) alloy has been evaluated at low and high strain rate shear deformation using a servo-hydraulic material testing machine and a Split Hopkinson Pressure Bar device, respectively. Microstructural studies were carried out as well to study the formation of adiabatic shear bands (ASB) using both optical and scanning electron microscopy.

1.1. Mechanical behavior of materials in shear

1.1.1. Shear stress and shear strain

Shear stress is a component of stress, which is defined by a vector parallel to the cross section of the material. As in Figure 1.1.a, two equal forces are applied on a bulk of the material in opposite directions. Layers of the material will slide over one another if the amount of force is high enough. [3]

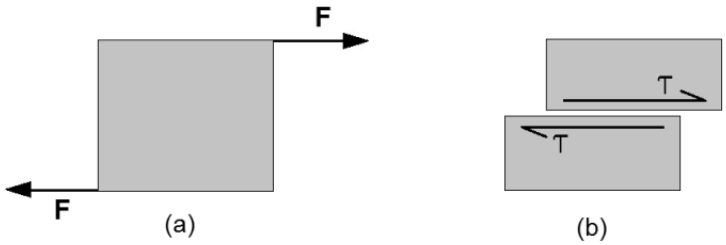

Figure 1.1. Deformation by shear

Shear stress is defined as the amount of force divided by the shear area. Equation (1) is used to calculate the shear stress, in which A is the area of the material resisting the shear.

$$\tau = \frac{F}{A} \tag{1}$$

The material changes its shape due to the shear stresses; therefore shear strain is defined as the angle of deformation as shown in Figure 1.2.

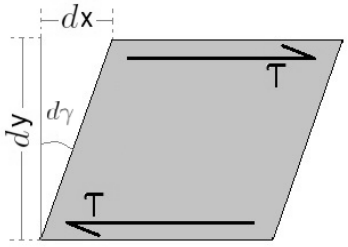

Figure 1.2. Shear strain

For small shear strains:

$$\tan\gamma \simeq \gamma \tag{2}$$

Therefore, according to Figure 1.2. shear strain can be calculated using Equation (3) .

$$d\gamma = \frac{dx}{dy} \tag{3}$$

1.1.2. Thermally activated dislocation motion

Dislocation motion is considered to be the main mechanism of plastic deformation in crystalline materials. The gliding of the dislocations is opposed by various obstacles, such as vacancies and grain boundaries. Therefore, the dislocation needs energy to overcome these barriers. The energy is provided either by externally applied stresses or by the internal energy of the atoms themselves (thermal vibration of atoms). As a result, the required shear stress depends on temperature and the deformation rate. Thermal activation is a dislocation motion mechanism up to strain rates of around 10^3 s^{-1}. At higher strain rates several dislocation drag mechanism are activated, which limit the dislocation motion and therefore affect the deformation. [4] [5]

Small particles, which can be overcome by thermal vibrations, are short range obstacles, such as cutting through small precipitates. However, if the energy barrier is extended over a large area, more energy is needed for the dislocation to overcome it. Therefore, there is a need for energy also from the externally applied stresses. These obstacles are called athermal, as the thermal energy is not enough to overcome them. The overall stress, which is required for the dislocation motion, can be calculated using Equation (4), in which σ_G is the stress needed for long range obstacles and σ^* indicates the stress for short range obstacles. [4] [5]

$$\sigma = \sigma_G + \sigma^* \tag{4}$$

The thermal vibration of atoms increases when the temperature is increased. Therefore, less energy is needed from the external stresses. Figure 1.3. illustrates the total energy to overcome the barriers as well as the share of thermal energy and external stress.

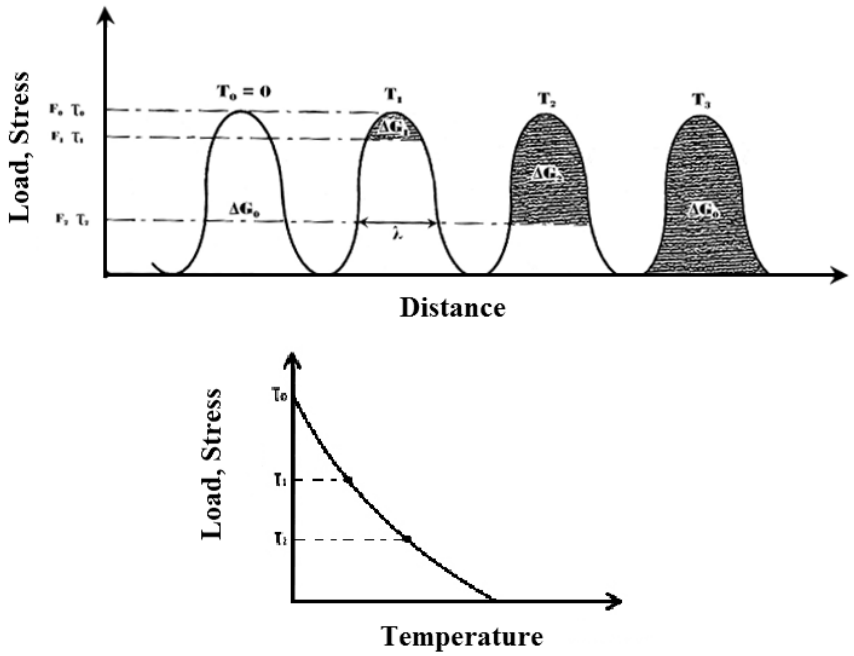

Figure 1.3. Thermal and mechanical energies required to overcome the energy barriers and corresponding external stresses at different temperatures, after [4]

Equation (5) expresses the probability that the momentary thermal energy is higher than the required thermal energy to pass the energy barrier. [4]

$$P_B = e^{\frac{-\Delta G}{kT}} \tag{5}$$

P_B is the probability, ΔG is the amount of thermal energy needed to overcome the obstacle, k is the Boltsman's constant, and T is the temperature. Based on Equation (5), the probability of a dislocation surmounting the barrier increases by increasing the available thermal energy and decreasing the amount of energy needed from the thermal energy.

1.1.3. Dependence of strain rate on thermal activation

The probability of a dislocation surmounting the barrier could also be defined as the ratio of the successful attempts of overcoming the obstacles to the total number of attempts. The number of attempts is proportional to the frequency. Therefore, if the vibration frequency of a dislocation is expressed by υ_0, then the frequency of successful attempts (υ_I) is defined as: [4]

$$\nu_I = \nu_0 e^{\frac{-\Delta G}{kT}} \tag{6}$$

The total time for a dislocation to glide a specific distance (Δt) consists of the time that dislocation moves in the free area between the obstacles (t_r) and the time that it waits for the thermal activation in front of an obstacle (t_w). The average waiting time depends on the probability of overcoming an obstacle. Therefore we can write:

$$t_w = \nu_I^{-1} = \nu_0^{-1} e^{\frac{-\Delta G}{kT}} \tag{7}$$

Equation (8) expresses the strain rate in the material. M is the orientation factor, ρ the dislocation density, and b is the Burgers vector. The dislocation velocity is $\Delta l/\Delta t$, in which Δl is the distance between two obstacles.

$$\frac{\partial \varepsilon}{\partial t} = \dot{\varepsilon} = (\frac{1}{M})\rho b \Delta l / \Delta t \tag{8}$$

Based on Equation (8), the dislocations have less time to wait and consequently less thermal activation at higher strain rates. As a result of this, the strength of the materials usually increases with increasing strain rate.

Equations (7) and (8) can be combined, and if:

$$\dot{\varepsilon} = \frac{\nu_0 \rho b \Delta l}{M} e^{\frac{-\Delta G}{kT}} \tag{9}$$

Then:

$$\Delta G = kT \ln \frac{\dot{\varepsilon}_0}{\dot{\varepsilon}} \tag{10}$$

From Equation (10) the effect of temperature and strain rate on the activation energy can be seen. Increasing the temperature and decreasing the strain rate increases the activation energy.

Figure 1.4. illustrates the effects of temperature and strain rate on the flow stress. As Equation (4) previously presented, the flow stress consists of two components (σ_G and σ^*). Above the critical temperature (T_c), the thermal energy is enough for the dislocations to overcome the barriers thermally activated and it does not affect the remaining long range barriers. Therefore the flow stress at this temperature consists of σ_G only. At lower temperatures more energy is required and the role of σ^* in the calculation of the flow stress becomes increasingly important. [4]

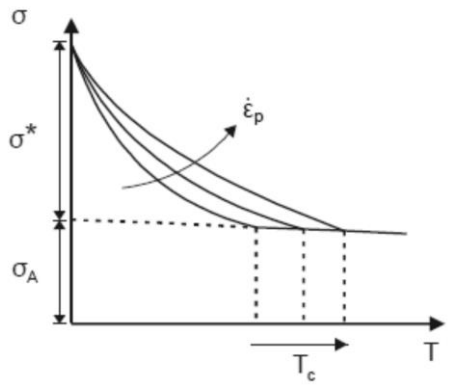

Figure 1.4. Flow stress as a function of temperature at different strain rates, after [4]

1.1.4. Dislocation drag

By increasing the strain rate the flow stress increases as well. Up to the strain rate of about 10^3 s^{-1}, the trend is rather steady. However, with further increase in the strain rate, a steep upturn appears in the flow stress vs. logarithmic strain rate. Figure 1.5. shows an example of this phenomenon for a stainless steel.

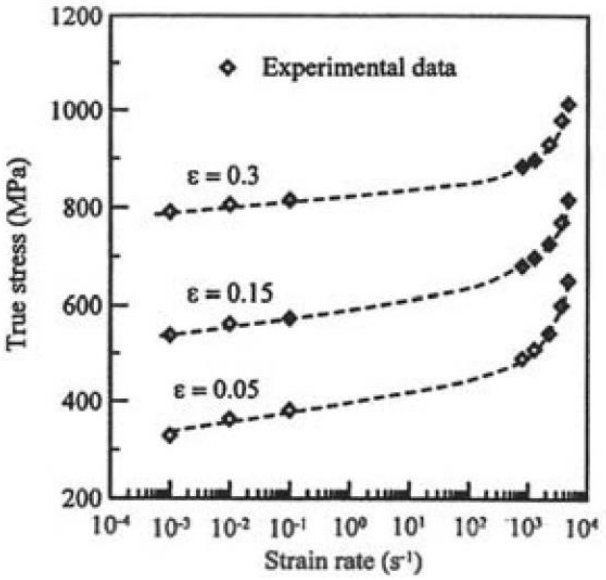

Figure 1.5. Flow stress vs. logarithmic strain rate for the AISI 304 stainless steel at three constant strains, after [4]

At high strain rates, several damping or viscous drag mechanisms are activated, which slow down the dislocation motion. Viscous drag consists of several mechanisms, such as phonon drag and emission of electrons, which dissipate the dislocation motion energy. The dislocation is accelerating and decelerating while moving by the externally applied stress, which will lead to phonon and electron emission. At higher dislocation velocities, the phonons start to interact with the dislocation. The emissions and interactions are consuming energy and thus opposing dislocation motion. Electron viscosity at lower temperatures and phonon viscosity at higher temperatures are the main opposing

mechanisms. As all these processes consume energy, more external energy is needed to keep the flow rate of the material constant. [4] [5]

1.1.5. Adiabatic heating

During plastic deformation a large portion of the applied energy is converted to heat. [6] Low strain rate tests in most cases are isothermal. This means that the heat generated by the plastic deformation does not increase the material's temperature, because the heat is conducted away from the deformation zone by the material. By increasing the strain rate the conditions change to adiabatic, as the duration of the deformation is short and the heat conducted by the material is negligible. [6] Therefore, the temperature of the material increases in the deformation zone during high strain rate deformations. The increased temperature leads to thermal softening of the deformation zone, which should be considered in the high strain rate testing as it lowers the material's strength [1]. Zener and Hollomon [7] first introduced this phenomenon for steel in 1944.

The rise in the temperature can be estimated using Equation (11), in which c and ρ are the heat capacity and density of the material, respectively. T is the shear stress and γ is the shear strain. β represents the fraction of the energy, which is transformed to heat and usually varies between 0.9-1. [8] If β=1, all the mechanical energy is converted to heat and no changes in the material microstructure take place (i.e. no energy is stored in the material). [4]

$$\Delta T = \frac{\beta}{\rho c} \int \tau d\gamma \tag{11}$$

1.2. Shear testing

The mechanical behavior of materials can be studied in various deformation modes. Different testing methods and standards are available for studying the material's behavior in tension and compression. Although there are different methods developed to study shear behavior as well, it is more challenging to design a mechanical test to evaluate the material's behavior in shear, due to various practical issues. It is also possible to convert the mechanical properties of isotropic materials from uniaxial testing to shear using analytical methods (e.g. von Mises, Tresca). However, in most of the cases it is necessary to study the shear behavior using experimental test methods. The material behavior in shear is strongly affected by the strain level, temperature, and strain rate, and therefore, various testing methods are being used to study the mechanical behavior of the materials in shear.

Torsion (rotational shear) tests provide valuable information about the mechanical properties of the material, such as the shear modulus, yield strength, and ultimate shear strength. These tests are usually carried out on cylinder or spool specimen. (Figure 1.6.) [9]

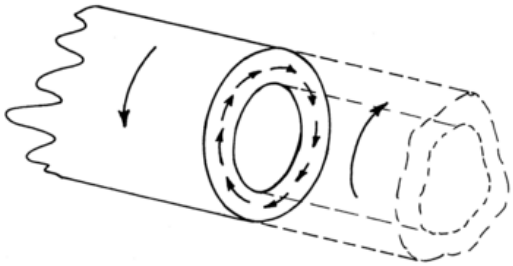

Figure 1.6. The orientation of rotational shear (torsion), [9]

In many techniques, the geometry of the specimen is modified in a way to produce shear deformation in uniaxial testing setups rather that designing a new complicated device to produce shear deformation. In translational shear tests, normal loading is applied to the specimens, which are designed to deform in shear. In other words, the normal stress is *translated* to shear stress. The translational shear tests consist of through-thickness tests and in-plane shear tests. (Figure 1.7.) [9]

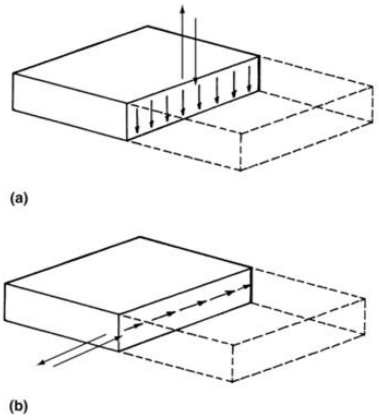

Figure 1.7. The orientation of translational shear, a) through-thickness, b) in-plane [9]

The through-thickness tests are designed to test the material's shear strength through the cross section. They can be performed as in single shear or double shear mode using different fixtures. (Figure 1.8.)

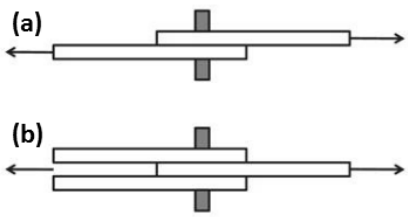

Figure 1.8.Through- thickness shear testing, a) single shear, b) double shear

The in-plane shear tests are used to study the shear anisotropy of materials in a sheet form. The specimen design is more complicated in these methods in comparison to the through-thickness tests. For instance Figure 1.9. presents a specimen design for double-notch shear test according to the ASTM standard. [10] When the specimen is loaded in tension or compression, the area between the notches goes through shear. The shear stress is then calculated based on the load and the geometry of the specimen. [9]

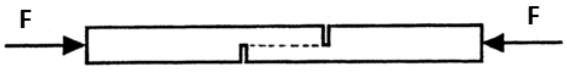

Figure 1.9. Schematic picture of a double-notch shear test specimen

In many industrial applications, the material undergoes high strain rate deformation. Therefore, it is crucial to study the mechanical behavior of materials also at high strain rates. High strain rate shear deformation occurs in various processes, such as ballistic impact, dynamic compression, explosive fragmentation, high speed shaping and forming, machining and grinding. [1] Therefore, there are various methods developed and modified to study the shear behavior at high strain rates. These methods are categorized based on the strain rate regime, at which they are performed. [11] (Table 1.2.)

At lower strain rates the most common technique is the servo-hydraulic machine modified to perform shear tests. In these machines a torsional actuator is used instead of a linear actuator in order to provide shear deformation. For intermediate strain rates, torsional impact testing is used. In this technique, a thin-walled tubular specimen is placed in a stationary support, which is loaded by a drive shaft with a desired angular velocity. [12] For higher strain rates the Split Hopkinson Pressure Bars and double-notch testing method are used. All these techniques are used to produce stress-strain curves in a wide

range of strain rates. A complete analysis of the shear behavior can be obtained by performing a combination of these tests at different strain rates. [11]

Table 1.2. Experimental methods for shear testing with their strain rate regimes, after [11]

Testing technique	Application strain rate (s^{-1})
servo-hydraulic frames	Up to 100
Torsional impact	10 to 10^3
Split Hopkinson bar	10^2 to 10^4
Double-notch shear	10^3 to 10^4

Many scientists have studied the mechanical behavior of materials in high strain rate shear using these methods. For instance, Khan et al. [13] have performed different tests to study the mechanical behavior of Ti-6Al-4V in wide ranges of strain rates (from quasi-static to dynamic regimes) and temperatures. Peirs et al. [14] have also studied the same material by performing both tensile and shear tests at high strain rates. Moreover, they have compared the experimental results with simulations to model the material's behavior.

1.2.2. Split Hopkinson Pressure Bar

The Split Hopkinson Pressure Bar (or Kolsky bar) technique (SHPB) is used to study the mechanical behavior of materials in the strain rate range of 10^2-10^4 s^{-1} in compression, tension, and shear. The technique is based on the propagation of elastic stress waves in solids. A SHPB set-up for compression consists of incident, transmission, and striker bars. A momentum trap bar can be added to the system to prevent reflection of the stress pulses back to the transmission bar. The bars, which have the same diameter, must be well aligned and usually are made of the same material. As in Figure 1.10., the specimen is placed between the pressure bars.

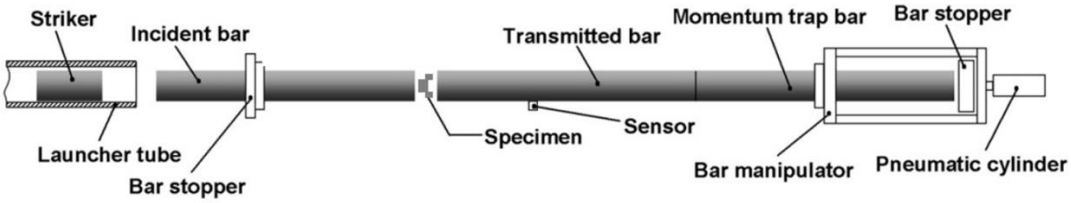

Figure1.10. Schematic picture of a SHPB setup, after [8]

The striker impacts the incident bar by suddenly released compressed air from the pressure tank. The resulting stress pulse travels through the bars and the specimen. With each impact three strain pulses are recorded by using strain gauges. The tress pulse is first produced in the incident bar. Part of this pulse is then transferred to the transmitted bar through the specimen (the transmission pulse) and part of it is reflected back to the incident bar (the reflected pulse). The specimen undergoes dynamic deformation during the movements of the stress pulse. The stress pulses are measured by strain gages, bonded to the bar surfaces, and recorded with proper instrumentation and a computer system attached to the device. The corresponding strain rate and stress-strain curve are obtained via proper calculations afterwards.

1.2.3. Hat-shaped specimens

Hat-shaped specimens are used to perform high strain rate shear deformation tests using the SHPB device. They were first introduced by Meyer and Manwaring in 1986. [15] In these specimens the deformation is localized in a narrow region, due to the geometry of the sample. These specimens are usually machined from a round bar, and they consist of a bar (the hat part) and a tube (the brim part), which are connected by a narrow ring. This region is the shear area, which compared to the rest of the specimen is rather small. This

allows the assumption that all the energy of the deformation is localized in the shear area. (Figure1.11.)

The specimen is placed between the incident and transmitted bars of the SHPB device. So with each impact, the hat part is forced into the brim part of the hat-shaped specimen, and the specimen goes through high strain rate shear. This method has been used to study the localization of shear stress by various scientists. [2] [15-19] For instance, Meyers et al. [2] have studied the microstructures after adiabatic shear localizations in the hat-shaped stainless steel specimens. They have performed high strain rate tests with SHPB up to 10^4 s^{-1}, followed by microstructural analysis. They have found the shear band width to be about 1-8 μm. Peirs et al. [16] as well have used hat-shaped specimens to study the high strain rate shear behavior of Ti-6Al-4V and have compared the experimental results to the simulated ones. They have categorized the deformation process in different levels: onset of strain localization, formation of ASBs, initiation and propagation of microcracks. They found the shear band width as an important parameter in their calculations.

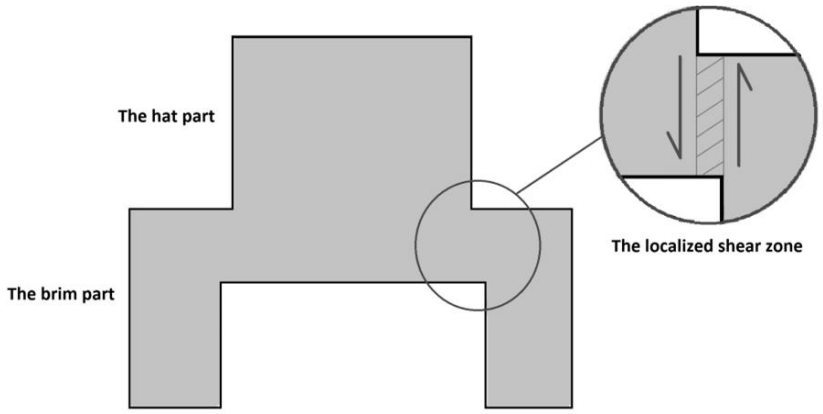

Figure 1.11. Schematic picture of the cross section of a hat-shaped specimen. The shear area is enlarged in the image

Stopper rings (or spacer rings) can be used to limit the amount of deformation in the hat-shaped specimens. The ring with the same outer diameter as the sample is placed around the hat part in the specimen. The rings are usually made of high strength material, and therefore they do not deform plastically. The stopper rings with different thicknesses can be used to study different amounts of shear displacement. Further microstructural analysis may be performed on the cross section of the deformed specimens to study the shear region. Lee et al. [17] have used the same method to limit the deformation of Ti-15Mo-5Zr-3Al in different stages in order to study correlation of the dynamic impact properties with adiabatic shear banding.

1.3. Adiabatic shear bands

Materials, especially metals, deform plastically because of shear stresses. Metals undergo dynamic shear loading in many industrial applications, such as forging, machining, and various impacts. During these events the deformation may lead to the formation of adiabatic shear bands and even fracture. [16] The shear bands are "narrow zones of intense plastic shear strain embedded in a homogeneously deforming region", as defined by Teng et al. [18] Although in most cases adiabatic shear bands lead to failure, they are not categorized as a failure mechanism. However, the material loses its load carrying and energy absorption capacity when adiabatic shear bands have formed. [16]

Formation of the adiabatic shear bands is a thermo-mechanical process, in which high amounts of deformation is localized in a narrow region within the material at high strain rates. [12] These shear bands (or slip bands) may form spontaneously within the bulk of the material during the deformation. For instance, Song et al. [19] have observed these slip bands in near-beta titanium alloy deformed at a high strain rate. Although it is possible to detect the slip bands in the micrographs of a deformed sample, it is not

practically possible to eliminate the effects of compressive stress on the formation of these bands. Therefore, it is necessary to study the shear bands as a result of shear stresses only.

Hat-shaped specimens are used to produce localized shear deformation in high strain rate testing, which in most cases results in the formation of adiabatic shear bands. [20] In other words, the deformation is *forced* into a narrow region in these kinds of experiments. Therefore, it is possible to investigate the shear bands by eliminating all other types of deformation, such as compression.

1.4. Titanium alloys

Titanium's superior physical and chemical properties have made it the best choice for many industrial applications. These properties, such as the excellent strength to weight ratio, corrosion resistance and relatively high melting point are achieved by present alloying elements. Titanium alloys have gained the attention of structural designers of the aerospace and chemical industries due to their properties, which justify the higher material and manufacturing costs. The elastic modulus of titanium is between that of steel and aluminum (about 110MPa), and in structural applications the maximum working temperature of titanium alloys is in the range of 425 to 580 °C. Formation of a passive TiO_2 layer on the surface of titanium-made parts provides high corrosion resistance. For the same reason, titanium resists the human fluids, and as it is nontoxic, it has become a good choice for biocompatible applications. [21]

Titanium alloy parts and components are produced using different methods: casting, wrought forms, and powder metallurgy. The first production step in all these methods is usually a double or triple melting procedure, using a vacuum electric furnace.

Two crystallographic forms of titanium exist: α-titanium with hcp structure and β-titanium with bcc structure. The transition temperature for pure titanium is 883 °C, which can be manipulated by alloying or thermo-mechanical processing. This allotropy leads to a wide range of alloys with different mechanical properties. The alpha alloys contain α-stabilizing elements, such as aluminum and tin, and have better creep resistance compared to the beta alloys. [21] Therefore, they are more used in high temperature applications. The alpha + beta alloys have a combination of the two phases, and their properties can be changed by heat treatments (via manipulating the amount and type of the β-phase). Ti-6Al-4V is the most common alloy of this type with many industrial applications. Finally, the beta alloys contain elements, such as vanadium or niobium, which decrease the α to β transition temperature. These alloys have better deformability and hardenability in comparison to alpha alloys. [21]

Table 1.3. Physical properties of Ti 15-3

Electrical resistivity μΩ.m	1.47
Thermal conductivity W/m.K	8.08
Density g/cm^3	4.71
Coefficient of linear thermal expansion μm/m (at 20-100 ºC)	8.5

Table 1.4. Mechanical properties of Ti 15-3

Tensile strength (Y_s) MPa	773
Ultimate tensile strength (UTS) MPa	785
Elongation (El) %	22

Ti 15-3 (or Ti 15-3-3-3) with a nominal composition of 15% V, 3% Al, 3% Cr, and 3% Sn is a commercial β titanium alloy, which is available in sheet, strip, and plate forms. It can be produced either as a wrought alloy or a cast alloy. It is a cold formable alloy even at room temperature. This property offers additional economic advantages for many

applications, such as producing thin sheets for composites. [22] It is also heat treatable to 1310 MPa of tensile strength. Due to its properties, Ti 15-3 is mainly used in high strength aircraft and aerospace components such as supersonic aircrafts. [23]

Tables 1.3. and 1.4. summarize some of the physical and mechanical properties of Ti 15-3 alloy according to ASM handbook. [23]

2. Experimental

This chapter introduces the studied materials, sample preparation methods, mechanical testing procedures and the microstructural studies. The mechanical testing was performed using the Split Hopkinson Pressure Bar (SHPB) device at high strain rates and a servo-hydraulic testing machine at low strain rates. The microstructural analyses were performed using both Optical Microscopy (OP) and Scanning Electron Microscopy (SEM).

2.1. Material

The material used in this study was a commercial metastable beta titanium alloy Ti-15-3-3-3. The nominal composition of the alloy is 15% vanadium, 3% aluminum, 3% chromium and 3% tin. The chemical composition of the material was also examined using EDS analysis. The results are presented in the next Chapter.

The material was prepared by Vacuum Arc Re-melting (VAR) and then forged to a 75 mm round billet using rotary swaging at 850 °C. The final step was to water quench the material from 700 °C to room temperature. No aging treatments were performed after the quenching, and the material was studied in the as-received condition.

The hat-shaped shear test specimens were machined using electric discharge machining. Figure 2.1. shows a side view picture of the sample.

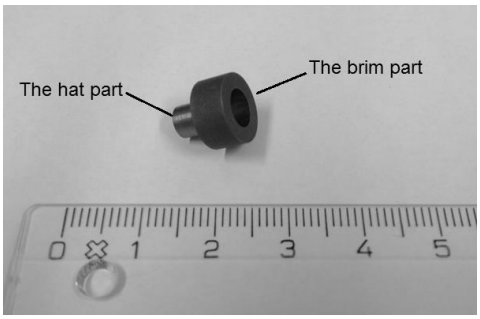

Figure 2.1. The hat-shaped specimen

A schematic picture of the sample and its dimensions are shown in Figure 2.2. In these specimens, three different regions can be identified: the hat part, the brim part, and the shear region, in which the shear stress (and strain) will be focused.

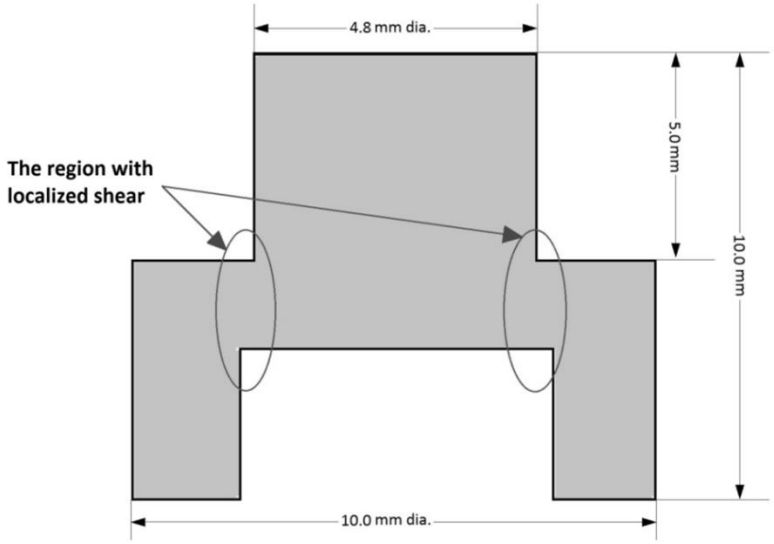

Figure 2.2. Schematic picture of the cross-section of the hat-shaped specimen

2.2. Mechanical testing

2.2.1. High strain rate testing

The SHPB device at the Department of Material Science of Tampere University of Technology was used to perform the high strain rate tests. (Figure 2.3.)

Figure 2.3. The SHPB device at Tampere University of Technology

The device used in this study consists of two pressure bars, incident and transmitted, with 22 mm diameter and 1200 mm length; as well as 3 striker bars with the same diameter and different lengths (200, 300, 400 mm). In addition, in this setup a third bar was used as a momentum trap to prevent the reflection of the transmitted pulse back to the transmitted bar. Figure 2.4. illustrates the SHPB setup as described, and Figure 2.5. shows the incident bar and the air gun used for accelerating the striker bar. All bars and strikers were made of high strength Maraging steel.

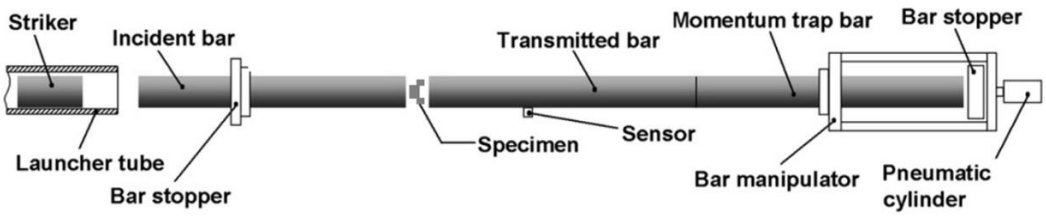

Figure 2.4. Schematic picture of the SHPB device (after [8]*)*

In this study, the high strain rate tests were performed at room temperature. The striker was shot with a sudden release of compressed air from the pressure container. The striker impacts the incident bar and generates a compressive stress pulse into the bar. In each test a thin copper disk was used as a pulse shaper to reduce the oscillations of the incident stress pulse. After the striker impacts the incident bar, the incident pulse travels in the bar towards the specimen, which is placed between the incident and transmitted bars. When the stress pulse reaches the specimen, part of the pulse transmits through the specimen to the transmitted bar (ε_t) and part of it reflects back (ε_r). All of these three stress pulses are recorded using strain gages bonded on the surfaces of the incident and transmitted bars. The signals are then amplified using a Kyowa CDV 700A signal conditioner and recorded by a high speed Yokogawa DL 708 digital oscilloscope. A computer is used to calculate the stress, strain, and strain rate in the specimen from the recorded signals using MATLAB.

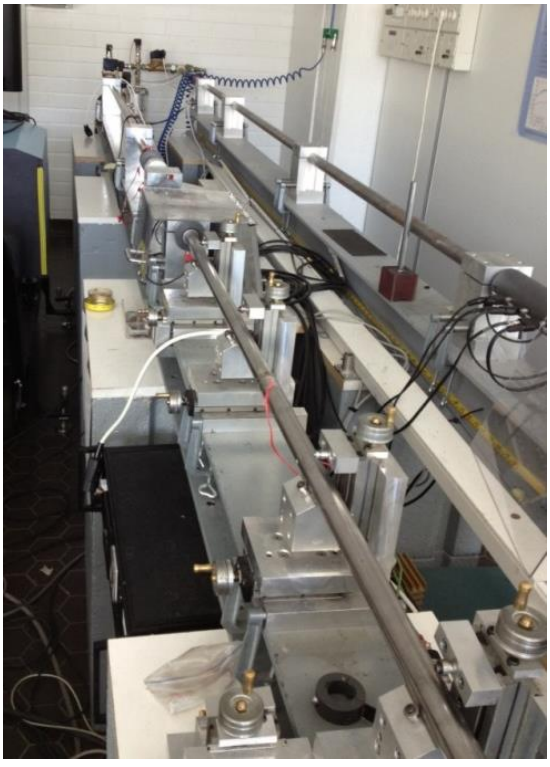

Figure 2.5. The incident bar and the air gun in the SHPB device

In this study, two series of tests were performed. In the first set of the tests, stopper rings were used to limit the amount of deformation. (Figure 2.6.) The stopper rings were machined from high strength steel, and therefore it was assumed that the amount of deformation in the stopper rings is negligible. The size (thickness) of the stopper ring determines the limit of deformation; therefore, four different stopper rings were used to study the material at various amounts of deformation. The thickness of the stopper rings ('t' in Figure 2.7.) were 1, 2, 3 and 4 mm.

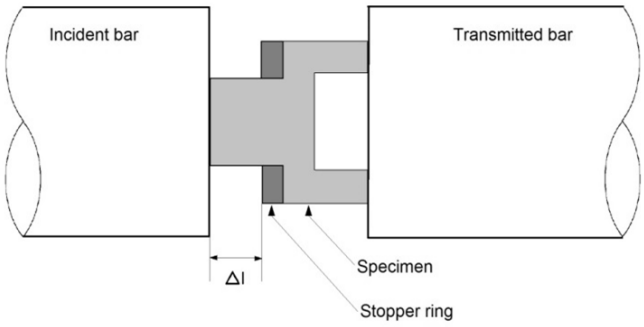

Figure 2.6. Schematic picture of the specimen positioning and the stopper rings in the SHPB device

This set of samples was later prepared for the microstructural studies in order to study the effects of deformation on the microstructure of the material and especially to determine the width of the primary shear band at different amounts of deformation.

In the second set of the tests, no stopper rings were used and the amount of deformation was not limited. The test results were used only to study the mechanical behavior of the material, i.e. the samples were not used for microstructural studies.

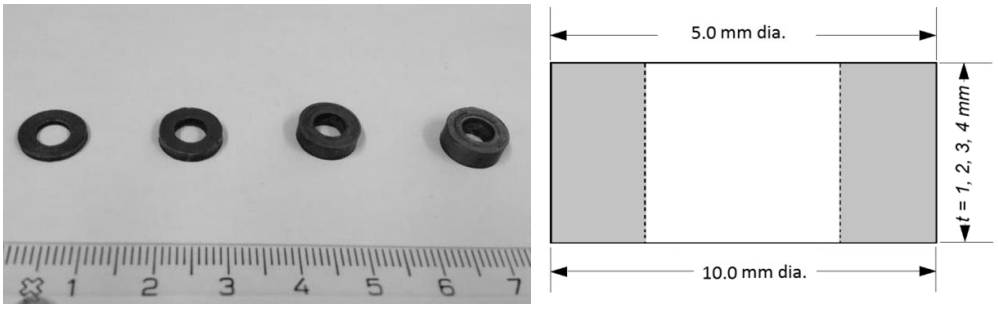

Figure 2.7. The stopper rings and their dimensions

2.2.2. Low strain rate testing

Two samples were tested using the servo-hydraulic materials testing machine (Instron 8800) to study the low strain rate behavior of the material. The tests were performed at crosshead speeds of 0.01 mm/s and 0.1 mm/s.

2.3. Microstructural studies

2.3.1. Sample preparation

The sample preparation was done for the samples of low strain rate mechanical test and the first set of samples (with stopper rings) at the high strain rate tests. Each specimen was cut in half using a rotating disc cutter (Struers Accutom-50) and hot-mounted into a polymeric resin using Struers CitoPress-10. The samples were ground using SiC grinding papers and diamond-polished using the schedule detailed in Table 2.1. After polishing, ultrasonic cleaning was used to clean the surface of the sample.

Table 2.1. The polishing procedure, after [24]

Polishing steps		
	Rough polishing	Fine polishing
Polishing cloth	MD-DAC	Micro-pad
Suspension	3µ diamond	1µ diamond
RPM	150	150
Force (N)	25	30
Time (min)	15	10

In the next step, the Kroll's reagent (Table 2.2.) was used to etch the surface of the specimens.

Table 2.2. Chemical composition of the Kroll's reagent

Kroll's reagent	
HF	1.5 ml
HNO_3	4 ml
H_2O	94 ml

The mounting resin was not conductive, and therefore the samples were carbon coated using Physical Vapour Deposition (PVD) for SEM analysis. The samples were also copper-taped before the SEM analysis.

2.3.2 OM and SEM analysis

Leica DM 2500 optical microscope was used to study the microstructure of each sample's cross section. The study was performed at magnifications ranging from 10x to 50x.

Some of the specimens were studied using the Philips XL-30 scanning electron microscope at 20 kV accelerating voltage for both Secondary Electron (SE) imaging and EDS analysis.

All OM and SEM images were studied using the Image Tool software. The software was used to measure the width of the shear bands. The measuring system of the software was calibrated using a scale bar.

3. Results and Discussion

This Chapter presents and discusses the results of the mechanical tests conducted both at the high strain rates with the SHPB and at the low strain rates with the servo-hydraulic testing machine. The microstructural images obtained with the optical microscope and the scanning electron microscope are also presented and discussed.

3.1. Microstructural analysis

3.1.1. EDS analysis

The EDS analysis was performed to obtain the chemical composition of the alloy. The results are presented in Figures 3.1. and 3.2. The chemical composition was found approximately the same as the nominal composition.

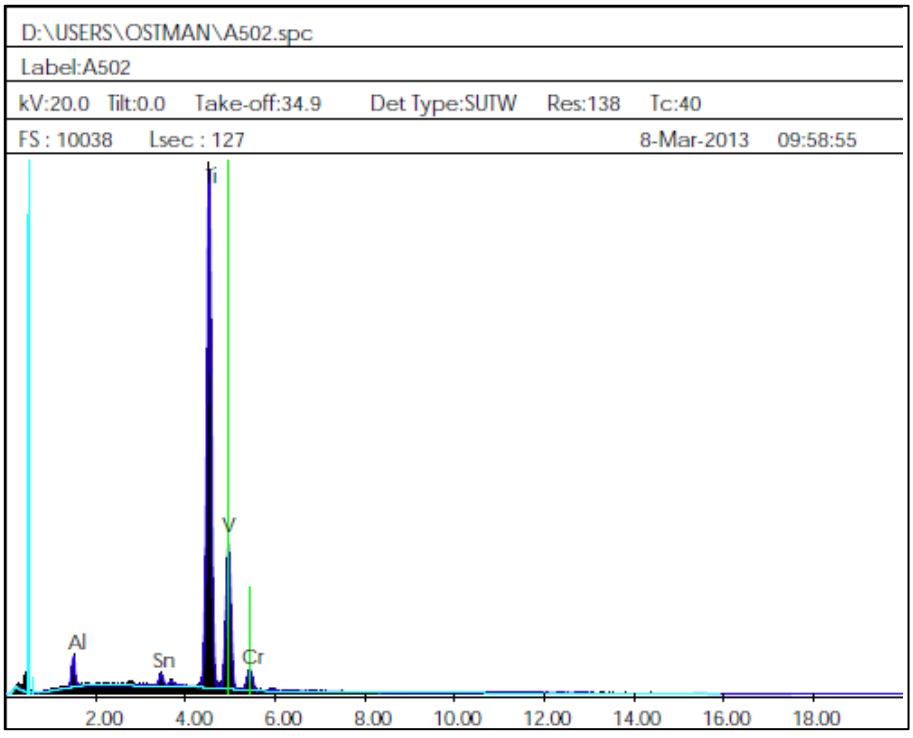

Figure 3.1. The EDS spectrum of the Ti-15-3-3-3 alloy

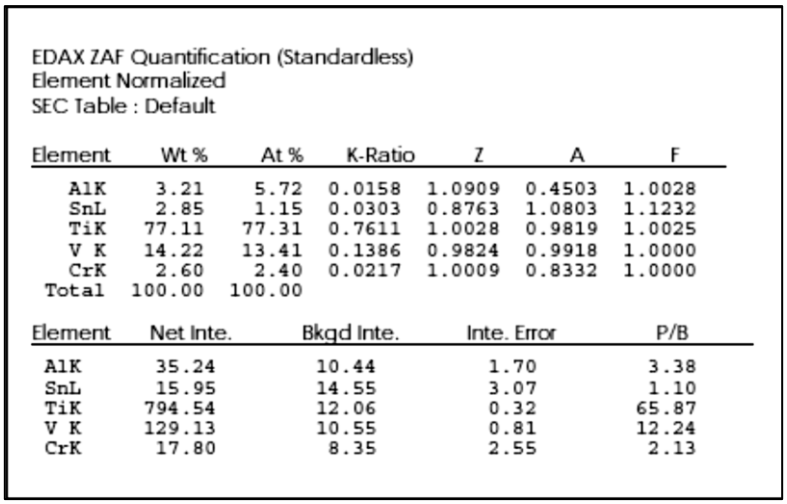

EDAX ZAF Quantification (Standardless)
Element Normalized
SEC Table : Default

Element	Wt %	At %	K-Ratio	Z	A	F
AlK	3.21	5.72	0.0158	1.0909	0.4503	1.0028
SnL	2.85	1.15	0.0303	0.8763	1.0803	1.1232
TiK	77.11	77.31	0.7611	1.0028	0.9819	1.0025
V K	14.22	13.41	0.1386	0.9824	0.9918	1.0000
CrK	2.60	2.40	0.0217	1.0009	0.8332	1.0000
Total	100.00	100.00				

Element	Net Inte.	Bkgd Inte.	Inte. Error	P/B
AlK	35.24	10.44	1.70	3.38
SnL	15.95	14.55	3.07	1.10
TiK	794.54	12.06	0.32	65.87
V K	129.13	10.55	0.81	12.24
CrK	17.80	8.35	2.55	2.13

Figure 3.2. The EDS analysis for the studied Ti-15-3-3-3 alloy

3.1.2. Microstructural analysis of the specimens deformed at high strain rate tests

The launch pressure and the length of the striker were controlled in the high strain rate tests, which both influence the speed of the striker. The striker velocity was recorded by the device software. Stopper rings were used to limit the amount of deformation in some of the tests. Table 3.1. summarizes the testing conditions of each sample in the first set of tests.

Table 3.1. Testing conditions for the first set of samples

Sample	Stopper ring thickness (mm)	Deformation Δl (mm)	Pressure (bar)	Striker length (cm)	Striker velocity (m/s)
S0	-	5	1	30	7.5
S1	1	4	1	30	4.8
S2	2	3	1	40	5.5
S3	3	2	1	40	6.0
S4	4	1	1	30	5.7
S5	1	4	4	40	16.6
S6	2	3	5	40	18.2

Figure 3.1. shows the cross section of an undeformed sample and of a sample deformed for 2 mm at the launch pressure of 3 bars and striker speed of 6 m/s. The average width of

the hat part in all specimens before testing was 4.78 mm (Figure 2.2). However, the average width of the hat part in the deformed samples after the high strain rate tests was 4.90 mm. The height and width of the hat parts were also measured from the macrographs shown in Figure 3.1. The hat part of the deformed sample is slightly shorter compared to that of the undeformed sample. Clearly the hat part was compressed during the deformation. However, in the mechanical behavior analysis of this material, i.e., calculation of the shear stress and shear strain, this compressive deformation was neglected to avoid unnecessary complications in the calculations. Therefore, all deformation was assumed to occur in the primary shear zone. The microstructural studies, as well, were mainly focused on the shear zone.

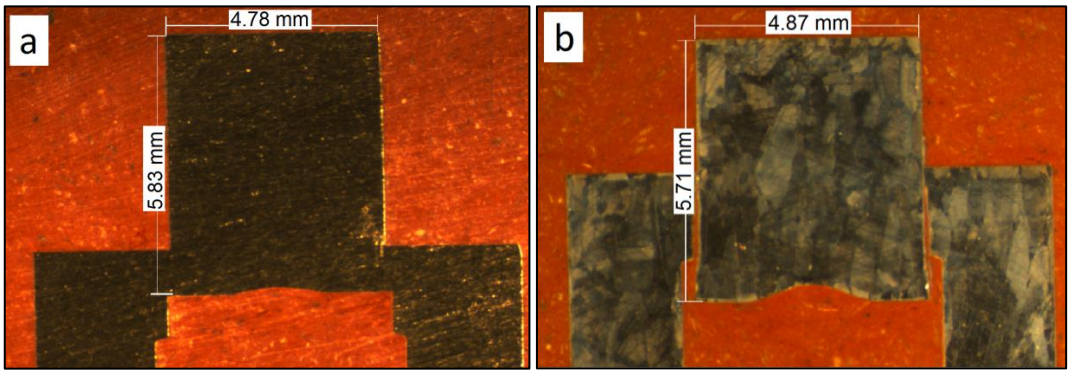

Figure 3.1.The cross section of a) an undeformed sample and b) a sample deformed for 2 mm at the launch pressure of 3 bar and the striker speed of 6 m/s

Hat-shaped specimens are widely used to study the localized shear, despite the assumption about the shear localization and the consequent probable errors in the calculations. Although other methods are available to study localized the shear and shear bands (such as thin-walled tubular specimens [12]), hat-shaped specimens are preferred due to their simple design and the transformation of compression to shear in them. (It is practically easier to perform compression tests and the facilities are readily available.)

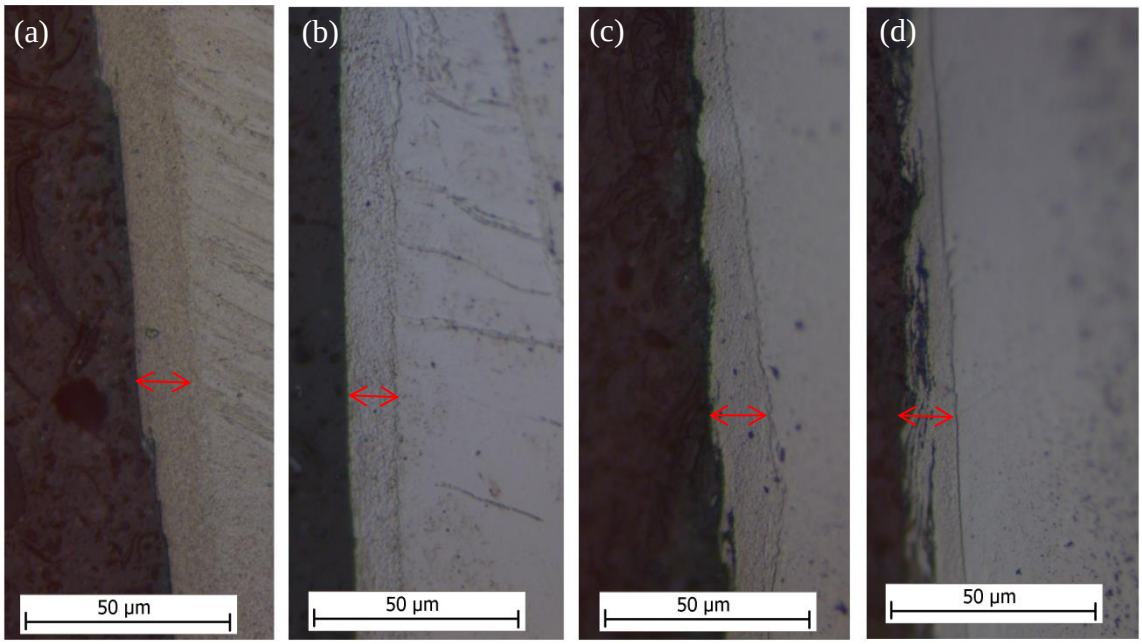

Figure 3.2. Optical micrographs of the primary shear zone in the hat part of the samples with a) 4, b) 3, c) 2, and d) 1 mm of deformation. The shear bands are marked in the images.

Figure 3.2. shows the optical microscope images of some of the samples. Different stopper rings were used to test these samples. Therefore, each sample is deformed to a different maximum displacement. The shear bands are easily observed in the micrographs. The shear band width was measured with Image Tool software from the OM images. Since the specimen fractures along the primary shear band, the shear band width was measured from the hat part and the brim part separately, and the total shear band width is the sum of these two values. The obtained total shear band widths are shown in Table 3.2. Despite the fact that the amount of deformation in the samples is different, the shear band width changes only slightly.

Although the shear bands can be clearly distinguished in the images, it is not easy to measure the width, since the thickness varies along the length of the shear band.

Therefore, the average of 20 measurements along the shear band was used as the total shear band thickness.

Table 3.2. The average shear band width obtained from the micrographs of the specimens deformed at high strain rates

Sample	Deformation, Δl (mm)	Striker velocity (m/s)	Average total shear band width (μm)
S2	3	5.5	16±3
S3	2	6.0	18±3
S4	1	5.7	18±4
S6	3	18.2	15±3

Some of the samples were studied using SEM as well. Figure 3.3. shows the SEM images of the shear zone and the shear bands at higher magnifications and better resolution for the sample deformed to (Δl) 3 mm at the launch pressure of 5 bar and striker velocity of 18.2 m/s. The measurements of the shear band width were performed also from the SEM images using the Image Tool software. The results were essentially identical to those obtained from the OM images. The shear band width at high strain rates and at the studied Δl values seems to be essentially independent of the amount of strain. Apparently the changes in the striker velocity have not affected the shear band width (Table B).

After studying all the samples, it was concluded that the shear band width is constant and essentially independent of the amount of deformation in the high strain rate regime. An average of the results in Table 3.2. (16.9 μm) was used in the calculations of the shear strains and strain rates.

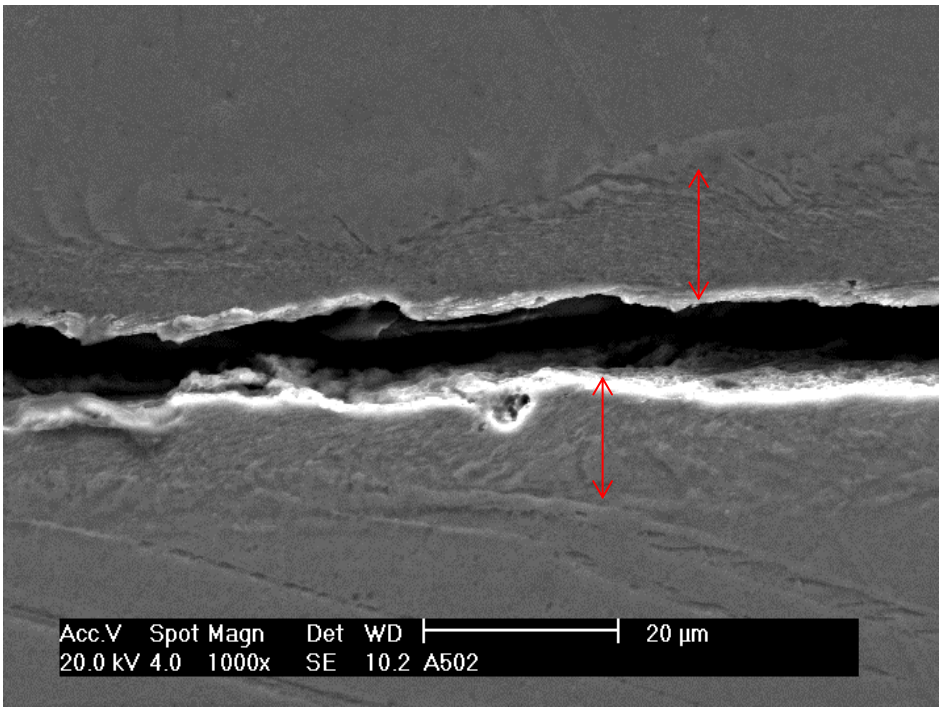

Figure 3.3. A SEM micrograph of the shear zone of a sample deformed to Δl=3mm using a launch pressure of 5 bar, and striker velocity of 18.2 m/s. The shear bands for both the hat and the brim part are marked in the image

3.1.3. Microstructural analysis of the specimens deformed at low strain rate tests

Figure 3.4. shows the cross sections of the samples tested with the displacement velocities of 0.01 m/s and 0.1 m/s. The shear bands were formed in the low strain rate tests as well. The shear band widths were measured in these samples from both the hat and brim parts similarly as for the specimens deformed at the high rates. The results are presented in Table 3.3. The shear band width increases with increasing displacement rate (and consequently the strain rate); while in the high strain rate tests the changes were negligible.

Table 3.3. The shear band widths for the low strain rate tests

Sample	Velocity (mm/s)	Average total shear band width (µm)
L1	0.01	26±6
L2	0.1	50±30

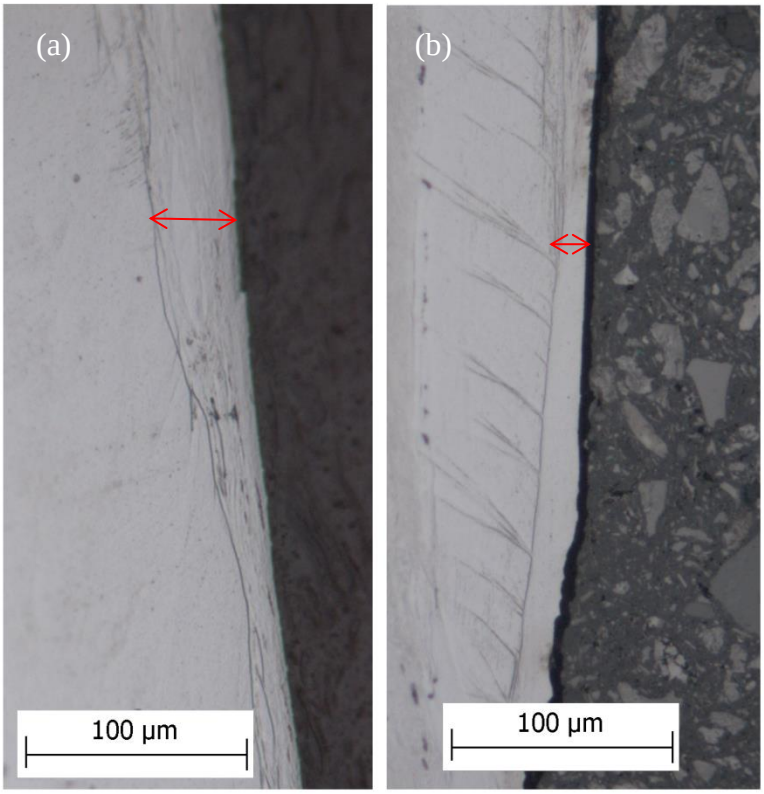

Figure 3.4. OM images of the cross sections of the samples tested at the displacement rates of a) 0.1 and b) 0.01 mm/s. The shear bands are marked in the images

In addition to the primary shear bands, also smaller individual slip bands can be seen in the microstructures of the specimens deformed at both low and high strain rate. Figure 3.5. shows SEM images of two specimens deformed at a high and at a low strain rate test. The secondary shear bands are marked in the image.

It is not in practice very easy to take the secondary shear bands into account in the shear band width measurements, mainly because there is no sharp line to clearly separate the secondary shear band from the rest of the material. These bands are a result of deformation that has occurred outside the primary shear zone.

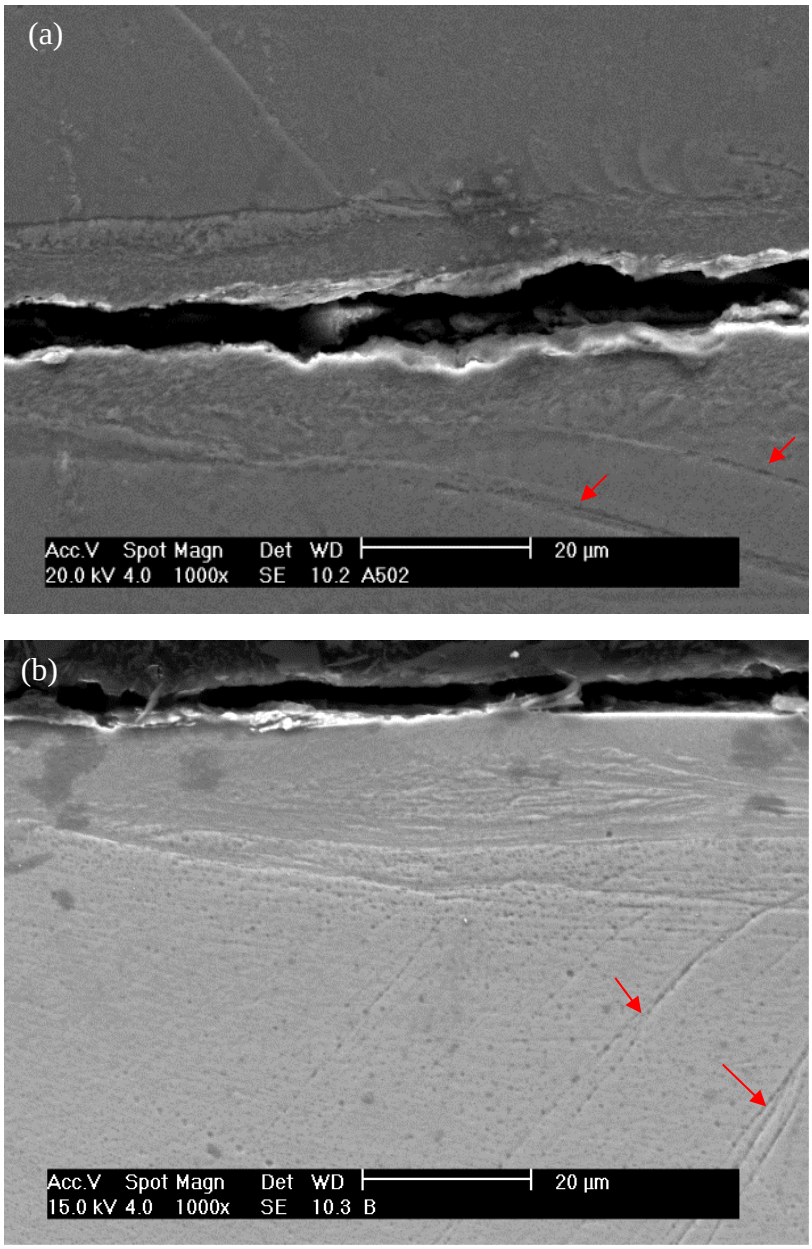

Figure 3.5. SEM images of a) a sample tested at with 5 bars pressure and to 3 mm of deformation and b) a low strain rate sample tested at 0.01 mm/s. Individual slip bands are marked in the image

The hat-shaped specimens were designed to localize the deformation in a narrow region between the hat and the brim parts. However, the deformation cannot be entirely focused in the shear zone due to the test conditions. The high strain rate and/or the rather high striker velocity may deform the sample also compressively in addition to the shear deformation. Therefore, the deformation expands to regions outside the primary shear

zone. However, it is still reasonable to assume that most of the deformation is localized in the narrow shear zone of the hat-shaped specimens because the amount of deformation in the shear zone is much higher in comparison to the rest of the sample.

3.2. Mechanical behavior analysis of the material

The mechanical properties of the material were studied using low and high strain rate mechanical tests. The shear stress, shear strain, and shear strain rate were calculated from the results of the mechanical tests.

Equation (12) was used to calculate the shear stress, in which F(t) is the load as a function of time and A is the shear area of the sample.

$$\tau(t) = \frac{F(t)}{A} \tag{12}$$

The shear area was calculated from the hat-shaped specimen geometry as in Equation (13), in which D is the diameter of the hat part and L is length of the shear zone.

$$A = LD\pi \tag{13}$$

Figure 3.6. shows the shear area in the specimen.

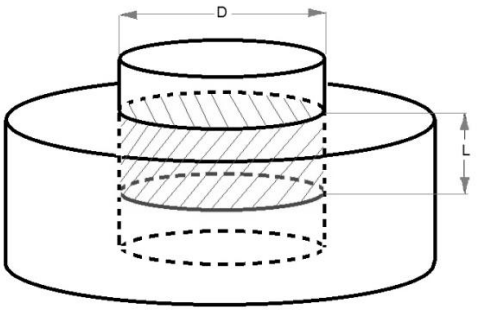

Figure 3.6. The shear area of the hat-shaped specimen

Calculation of the shear strain is more complicated. Figure 3.7. shows a schematic picture of the shear zone in the sample before and after deformation. The shape of the shear zone changes during the deformation, and this transformation is used to calculate the shear strain.

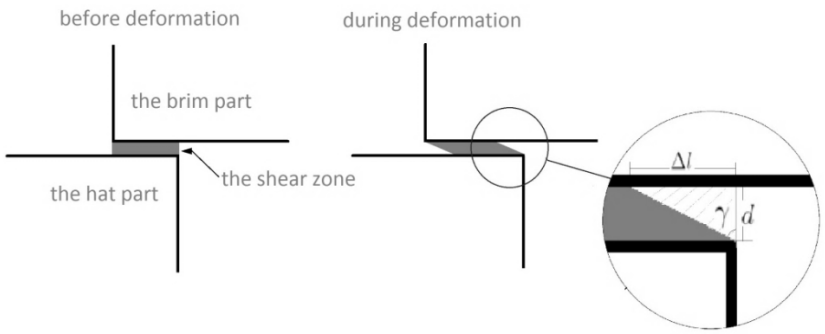

Figure 3.7. Schematic picture of the deformation of the shear zone in the hat-shaped specimen

The hatched triangle in Figure 3.7. shows the shear strain based on the definition. Δl is the displacement, d is the shear band width obtained from microstructural analysis, and γ is the shear strain.

Equation (14) can be obtained from Figure 3.7. The shear band width (d) is constant, and therefore, the shear strain can be simply obtained using Equation (14).

$$\gamma(t) = \frac{\Delta l(t)}{d} \tag{14}$$

3.2.1. Mechanical behavior analysis of the material at low strain rate tests

Equation (15) is used to calculate the strain rates in the low strain rate tests.

$$\dot{\gamma} = \frac{d\gamma}{dt} \tag{15}$$

Having $\gamma(t)$ calculated from Equation (14) and the displacement rate denoted by V, the Equation (15) can be rewritten as Equation (16), in which d is the shear band width from Table 3.3.

$$\dot{\gamma} = \frac{V}{d} \tag{16}$$

Table 3.4. presents the strain rates calculated using Equation (16).

Table 3.4. Strain rate in the low strain rate tests

Sample	Velocity (mm/s)	Strain rate (1/s)
L1	0.01	0.4
L2	0.1	2

The shear stress-shear strain curves are presented in Figure 3.8. The shear stress and shear strain were calculated for both low strain rate tests using the Equations presented in the previous Section.

From Figure 3.8. it is seen that in low strain rate tests the material's response begins with pure elastic deformation. The shear modulus (G) values obtained from the determined shear stress-shear strain curves are G_1= 0.10 GPa and G_2= 0.33 GPa for the strain rates of 0.4 s^{-1} and 2 s^{-1}, respectively. However, for Ti15-3 alloy G is known to be about 30-40 GPa depending on the heat treatment. [25] This indicates that the elastic parts of the shear stress-shear strain curves in Figure 3.8. cannot be used to determine the shear modulus of the material. As described earlier, the shear strain in this work was calculated using the displacement (Δl) and shear band width (d); the displacement being measured during the tests by the LVDT (Linear Variable Differential Transformer), which is not precise enough for the determination of the shear module. On the other hand, the shear band

width was measured from the micrographs after the tests with an assumption that all the deformation is localized in the primary shear bands. Therefore, the calculated shear moduli in these experiments differ clearly from the true values measured with more precise systems.

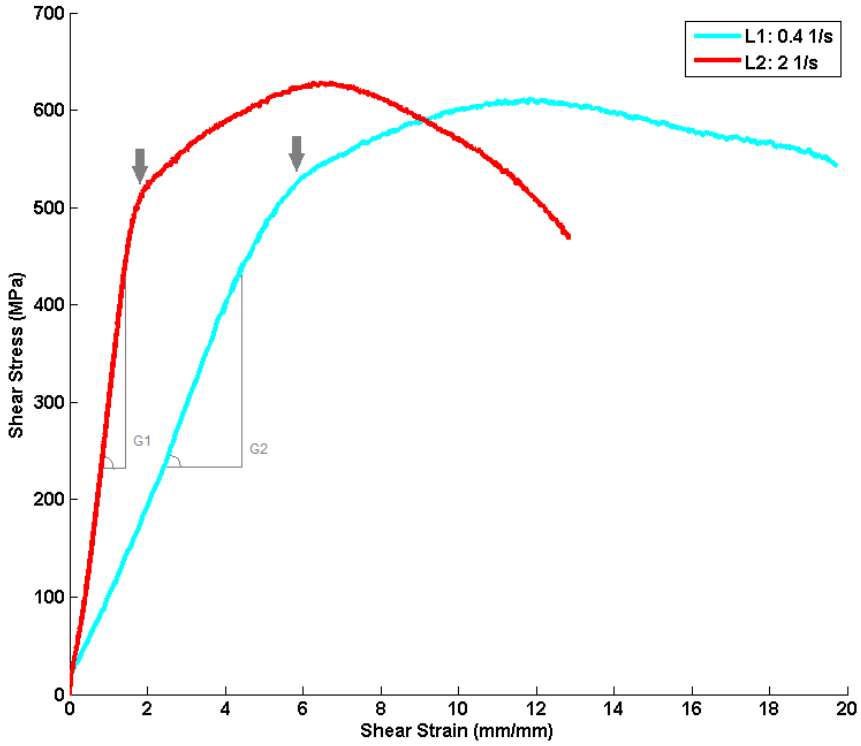

Figure 3.8. Shear stress vs. shear strain for the low strain rate mechanical tests. The shear modulus and yield point are marked in the image

The yield points for both tests are marked in the image. After the yield point the plastic deformation starts. Strain hardening occurs in these samples during the plastic deformation, which is seen as an increasing slope in the shear stress-shear strain curve. The deformation most probably expands through the shear zone as the material is strain hardening during the deformation. Therefore, it can be concluded that the shear bands were expanded during the strain hardening of the material.

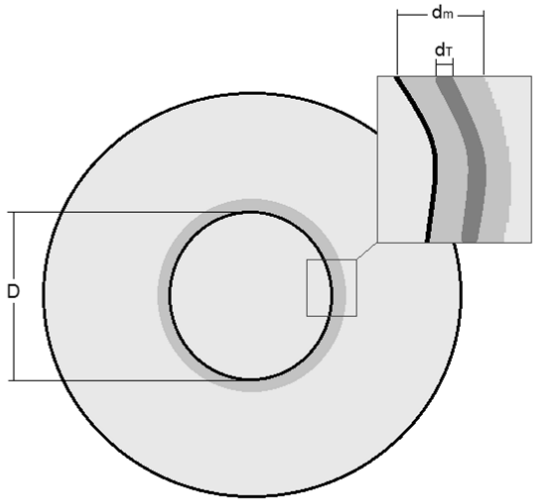

Figure 3.9. A schematic top view of the hat-shaped specimen with an enlarged image of the shear band width. D is the hat part diameter, dm is the measured shear band width, and dT is the true shear band width after localization

After a certain amount of deformation, the shear stress is not equally distributed along the shear band width, and most probably it is localized in a narrower region. (Figure 3.9.) Therefore, the shear area changes as the true diameter of the hat part is changing. The true width of the shear bands (d_T) is decreasing as well. This is believed to be the reason of the slope change in Figure 3.8.

3.2.2. Mechanical behavior analysis of the material at high strain rate tests

Table 3.5. shows the launch pressures used in the second set of the tests. A 20 cm striker was used in all tests.

Table 3.5. Test conditions for the second set of samples

Sample	Pressure (bar)	Striker velocity (m/s)
T1	1	9.1
T2	2	16.1
T3	3	20.4
T4	4	23.7

The data was collected and recorded from each high strain rate test. The incident (ε_i), reflected (ε_r), and transmitted (ε_t) strain pulses were recorded as a function of time. The following calculations were done to evaluate the shear stress vs. shear strain behavior of the tested material.

The velocity of the ends of the incident and transmitted bars was calculated using Equations (17) and (18), where C is the speed of sound in the bar material. For the Maraging steel bars, C is 4838 m/s.

$$V_T(t) = C\varepsilon_T(t) \tag{17}$$

$$V_I(t) = C(\varepsilon_I(t) - \varepsilon_R(t)) \tag{18}$$

The displacement was calculated by integrating the velocities over time. (Equation (19))

$$\Delta l(t) = \left| \int_0^t V_I(s)ds - \int_0^t V_T(s)ds \right| \tag{19}$$

Having the Δl calculated, the shear strain was calculated using Equation (14).

Figure 3.10. shows the shear strain vs. time plots obtained from the tests. The strain rate is the slope of the linear region of the curves. The strain rates obtained from Figure 3.10. are shown in Table 3.6.

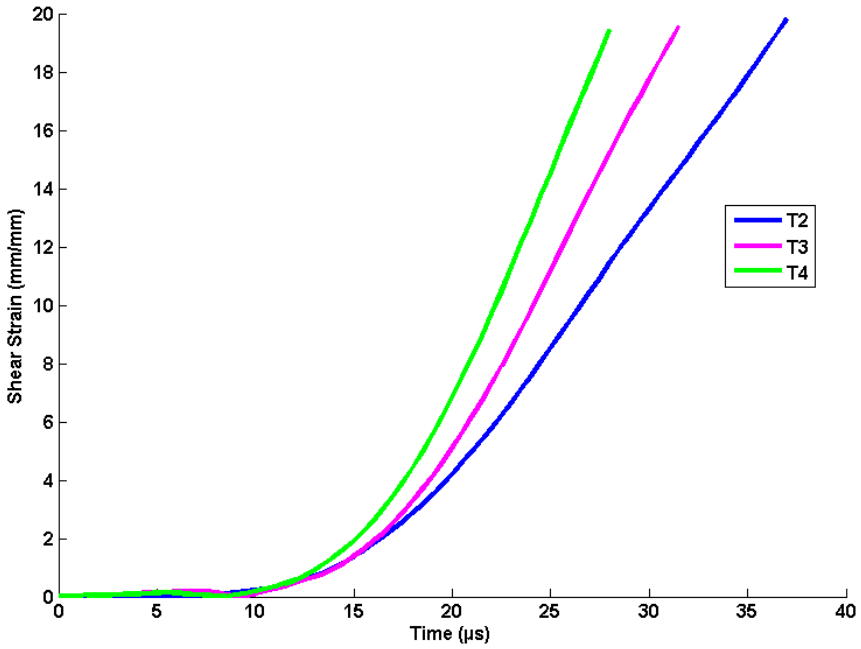

Figure 3.10. The shear strain vs. time

Table 3.6. Strain rates in tests shown in Figure 3.10.

Test	Strain rate x 10^6 (s^{-1})
T2	1.6
T3	1.3
T4	0.9

Equation (20) was used to calculate the load. In the Equation E_{bar} is the Young modulus and A_{bar} is the cross sectional area of the bars. In this device A_{bar} and E_{bar} are 3.722 cm^2 and 209.180 GPa, respectively.

$$F(t) = \varepsilon_T(t) E_{\text{bar}} A_{\text{bar}} \tag{20}$$

Having the load calculated, the shear stress was calculated using Equation (12).

Figure 3.11. shows the shear stress vs. shear strain curves for this set of samples. The material behaves again elastically at lower shear strains. After the elastic region, a sharp

peak appears in the shear stress-shear strain curves. Before the final failure, the material tends to respond with decreasing shear stress while the amount of shear strain is increasing.

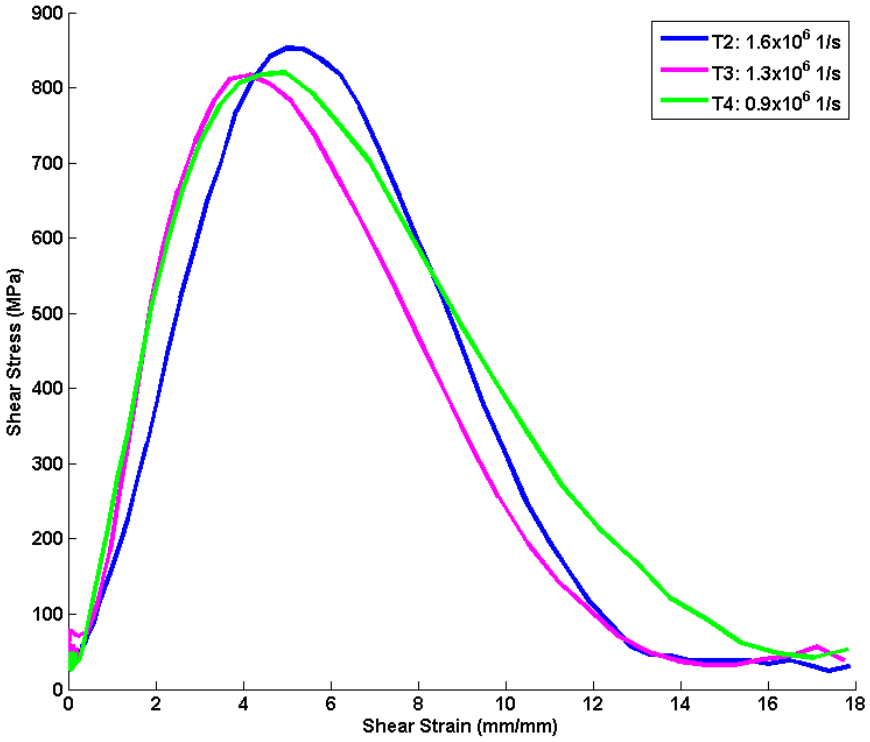

Figure 3.11. Shear stress vs. shear strain for the high strain rate tests

3.2.3. Comparison of the mechanical behavior of the material at low and high strain rate tests

Figure 3.12. shows the shear stress – displacement curves obtained from both low and high strain rate tests. The mechanical behavior of the material is clearly different in the high and low strain rate tests.

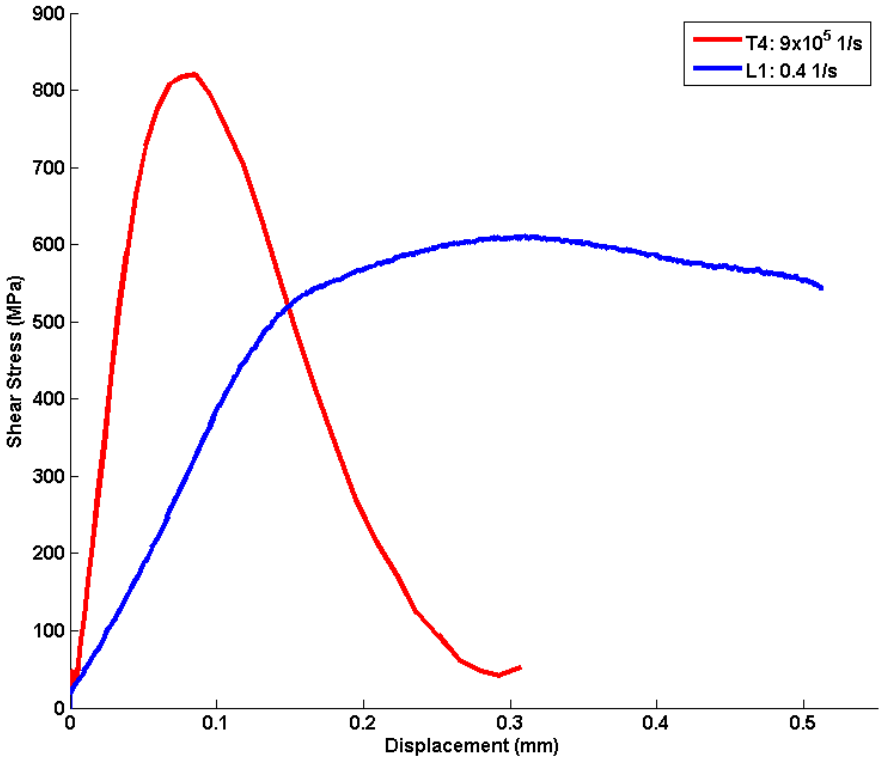

Figure 3.12. Shear stress vs. displacement curves obtained at the strain rates of $9x10^5\ s^{-1}$ and $0.4\ s^{-1}$

The plastic deformation in low strain rate test starts after the elastic region. The yield point can be detected approximately at about 0.15 mm of displacement. However, for high strain rate test, it is not possible to clearly distinguish between the elastic and the plastic regions as there is no clear slope change in the curve. Although the exact yield point cannot be detected in the high strain test, it is evidently before the maximum stress point in the curve.

After the elastic region a sharp peak appears in the shear stress-displacement curve of the high strain rate test, whereas in low strain rate tests a wide maximum point appears at much higher displacements. The maximum shear stress is clearly higher than the maximum shear stress observed in the low strain rate tests, and it occurs at smaller displacements. Peirs et al. [16] have reported similar high strain behavior for Ti-6Al-4V.

3.2.4. Adiabatic heating in high strain rate shear

Adiabatic heating happens in the high strain rate tests. It is not possible to measure the temperature directly but the temperature change can be calculated using Equation (21).

$$\Delta T = \frac{\beta}{\rho c} \int \tau d\gamma \tag{21}$$

in which T and γ are the shear stress and shear strain, respectively. ρ and c are the density and special heat capacity of the material, which are 4.76 g/cm^3 and 0.069 J/kg.k. β is the fraction of mechancial energy, which is converted to heat. β=1 means all the mechanical energy of the impact is converted to heat. In this work β was chosen to be 0.9.

Assuming that all the deformation is focused in the shear zone, the temperature in the shear band can be estimated using Equation (21). The calculated temperatures are shown in Table 3.7. The estimated temperatures are relatively high compared to the melting point of titanium (≈1670 °C).

Table 3.7. The estimated increase of temperature

Sample	ΔT (°C)
T1	1381
T2	982
T3	763
T4	840

Figure 3.13. shows how the temperature is increasing while the material is deforming in high strain rate shear based on Equation (21).

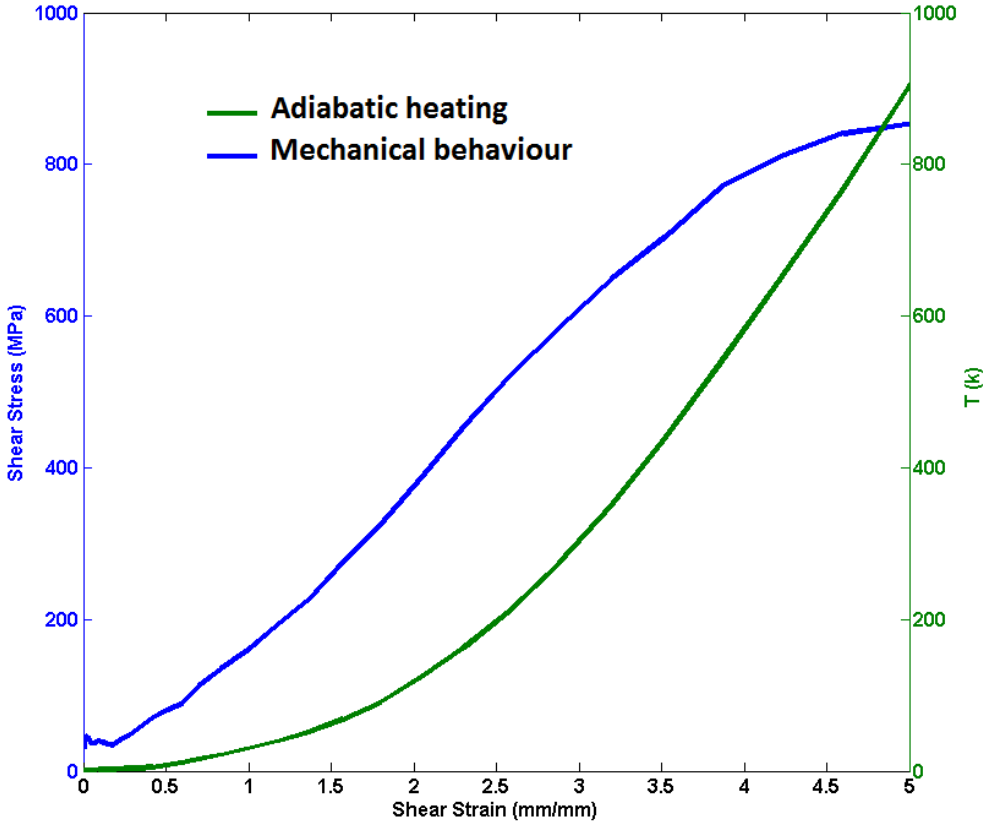

Figure 3.13. Shear stress and adiabatic heating as a function of shear strain at the strain rate of $1.6x10^6$ s^{-1}

The adiabatic heating leads to thermal softening of the deformation zone which decreases the strength of the material. On the other hand, strain hardening increases the strength. Normally, the shear bands expand if the strain hardening is strong. However, if the thermal softening is stronger than the strain hardening, the deformation will quickly localize and the shear band thickness remains constant. Ranc et al. [6] and Teng et al. [18] have suggested the same explanation for the formation of the shear bands. Their studies, however, do not focus on the constant shear band width. This explanation can justify the shear stress-displacement curves as well (Figure 3.12.). Strain hardening most probably would have appeared as an increasing slope in the shear stress-displacement curve, if its effects were not weakened by thermal softening. The high strain rate impact should result

in a high amount of strain hardening; however the simultaneous thermal softening weakens its effect. [19] [6]

4. Summary and Conclusions

The objective of this thesis was to study the adiabatic shear banding in titanium 15-3-3-3 alloy. This commercial titanium alloy is mostly used in aircraft and aerospace industries. The mechanical behavior of the material was studied both at low and high strain rates. The low strain rate mechanical tests were performed using a servo-hydraulic testing machine, and the high strain rate tests were done using the Split Hopkinson Pressure Bar device. Hat-shaped specimens were used to study the shear behavior of the material. These specimens localize the deformation in a narrow region due to their special geometry. As a result of this, the shear stress is focused into a small region in the sample, which leads to the formation of adiabatic shear bands at higher strain rates. Stopper rings with different thicknesses were used to limit the displacement (and consequently the deformation) to different amounts in some samples. The samples were then cut in half, mounted, and prepared for microstructural studies. Optical and scanning electron microscopes were used to evaluate the shear band formation in the shear zone for some of the samples.

Shear band formation was observed in the high strain rate tests (0.9-1.6 x 10^6 s^{-1}) as well as in the low strain rate tests (0.4 and 2 s^{-1}). The widths of the shear bands were measured from the micrographs using the Image Tool software. The shear band width was found almost constant for the high strain rate tests with different testing conditions (different amount of displacement and striker velocity) unlike in the low strain rate tests. Therefore, this constant value (16.9 μm) was used in the calculations of the strain and strain rate. The shear stress and shear strain were calculated for some of the tests. The shear stress - shear strain curves were plotted for both low and high strain rate tests to study the shear behavior of the material.

In the low strain rate tests, the material shows an elastic behavior for lower amounts of strain, and after the yield point the strain hardening starts as an increasing slope in the shear stress - shear strain curve. Finally the material starts to fail after a certain amount of deformation.

However, the mechanical behavior of the material was found rather different in the high strain rate tests. The material response again starts with elastic deformation, but it reaches a higher maximum shear stress in a lower amount of displacement. Strain hardening occurs in the material at high strain rates as well, but it cannot be observed in the shear stress-displacement curve due to adiabatic heating effect.

Adiabatic heating occurs in the shear zone of the samples tested at high strain rates due to the localization of shear strain. This heating results in the thermal softening of the material, which weakens the effect of strain hardening. The strain hardening also tends to increase the shear band width, while thermal softening tends to decrease it. This simultaneous strain hardening and thermal softening is believed to be reason for the different shear stress - shear strain curves as well as for the constant shear band width.

5. References

[1] D. Yang, Y. An, P. Cizek, P. Hodgson, "Development of adiabatic shear band in cold-rolled titanium," *Material Science and Engineering A,* vol. 528, no. 12, pp. 3990-3997, 2011.

[2] M.A. Meyers, Y.B. Xu, Q. Xue, M.T. Perez-Prado, T.R. McNelly, "Microstructural evolution in adiabatic shear localization in stainless steel," *Acta Materialia,* no. 51, pp. 1307-1325, 2003.

[3] G. E. Dieter, Mechanical Metallurgy, McGraw-Hill, 1976.

[4] M. A. Meyers, Dynamic Behaviour of Materials, USA: Weily , 1994.

[5] M. Hokka, Doctoral thesis: Effect of strain rate and temperature on the mechanical behavior of advanced high strength steel, Tampere: Tampere University of Technology , 2008.

[6] N. Ranc, L. Taravella, V. Pina, P. Herve, "Temperature field measurement in titanium alloy during high strain rate loading—Adiabatic shear bands phenomenon," *Mechanics of Materials,* vol. 40, no. 4-5, pp. 255-270, 2008.

[7] C.Zener, J. H. Hollomon, "Effect of strain rate upon plastic flow of steel," *Applied Physics,* vol. 15, no. 1, pp. 22-32, 1944.

[8] M. Hokka, T. Leemet, A. Shrot, M. Baeker, V.-T. Kuokkala, "Characterization and numerical modeling of high strain rate mechanical behavior of Ti-15-3 alloy for

machining simulations," *Material Science and Engineering A*, no. 550, pp. 350-357, 2012.

[9] H.A.Kuhn, "Shear, torsion and multiaxial testing," *Mechanical Testing and Evaluation, ASM international Handbook, vol.8*, pp. 185-194, 2000.

[10] "ASTM International," USA, 2013. [Online]. Available: http://www.astm.org/.

[11] S.Nemat-Nasser, "In troduction to high strain rate testing," *Mechanical Testing and Evaluation, ASM Handbook, ASM International*, vol. 8, pp. 447-461, 2000.

[12] J. D. Shih-Chieh Liao, "Adiabatic shear bands in Ti-6Al-4V titanium alloy," *Mechanical Physics of Solids*, vol. 46, no. 11, pp. 2201-2231, 1998.

[13] Akhtar S. Khan, Rehan Kazemi, Babak Farrokh, "Multiaxial and non-proportional loading responses, anisotropy and modeling of Ti-6Al-4V titanium alloy over wide range of strain rate and temperatures," *International Journal of Plasticity* , no. 23, pp. 931-950, 2007.

[14] J. Peirs, P. Verleysen, W. Van Paepegem, J. Degrieck, "Determining the stress-strain behavior at large strains from high strain rate tensile and shear experiments," *International Journal of Impact Engineering*, no. 38, pp. 406-415, 2011.

[15] LW Meyer, S. Manwaring, "Critical adiabatic shear strength of low alloyed steel under compressive loading," in *Metallurgical applications of shock-wave and high strain rate phenomena*, New York, Marcel Dekker Inc. , 1986, pp. 657-674.

[16] J. Peris, P. Verleysen, J. Degrieck, F. Coghe, "The use of hat-shaped specimenas to study the high strain rate shear behaviour of Ti-6Al-4V," *International Journal of*

Impact Engineering, no. 37, pp. 703-714, 2010.

[17] Woei-Shyan Lee, Chi-Feng Lin, Tao-Hsing Chen, Hsin-Haw Hwang, "Correlation of dynamic impact properties with adiabatic shear banding in Ti-15Mo-5Zr-3Al alloy," *Material Science and Engineering A,* no. 475, pp. 172-184, 2008.

[18] x. Teng, T. Wierzbicki, H. Couque, "On the transition from adiabatic shear banding to fracture," *Mechanichs of Materials,* no. 39, pp. 107-125, 2007.

[19] Wei Qian Song, Shoujin Sun, Suming Zhu, Gui Wang, James Wang, Matthew S. Dargusch, "Compressive deformation behavior of a near-beta titanium alloy," *Materials and Design,* no. 34, pp. 739-745, 2012.

[20] D. Rittel, Z.G. Wang, A. Dorogoy, "Geometrical imperfection and adiabatic shear banding," *International Journal of Impact Engineering,* vol. 35, no. 11, pp. 1280-1292, 2008.

[21] J. Destefani, "Introduction to Titanium and Titanium alloys," *ASM Handbook, ASM International* , vol. 2, pp. 586-591, 1990.

[22] Z.N. Ismarrubie, Aidy Ali, T. Satake, M. Sugano, "Influance of microstrudture on fatige damage mechanisms in Ti-15-3 alloy," *Materials and Design* , vol. 32, no. 3, pp. 1456-1461, 2011.

[23] S. Lampman, "Wrought Titanium and Titanium Alloys," *ASM handbook, ASM International* , Vols. 2, Properties and Selection: Nonferrous Alloys and Special-Purpose Materials, pp. 592-633, 1990.

[24] G. F. Vander Voort, Buehler Ltd., "Titanium specimen preparation," *Advanced*

Matreials and Processes, pp. 25-27, 2008.

[25] "Matweb, Material property data," Matweb, LLC, [Online]. Available: http://www.matweb.com.

[26] Y.Yang, F. Jiang, B.M. Zhou, X.M. Li, H.G. Zheng, Q.M. Zhang, "Microstructural characterization and evolution mechanism of adiabatic shear band in near beta-Ti alloy," *Material Science and Engineering A*, no. 528, pp. 2787-2794, 2011.

[27] B.F. Wang, Y. Yang, "Microstructure evolution in adiabatic shear band in fine-grain-sized Ti-3Al-5Mo-4.5V alloy," *Materials Science and Engineering A*, no. 473, pp. 306-311, 2008.

[28] Su-Tang Chiou, Hsien-Lung Tsai, Woei-Shyan Lee, "Effects of strain rate and temperature on the deformation and fracture behavior of titanium alloys," *Materials Transactions* , vol. 48, no. 9, pp. 2525-2533, 2007.

[29] Q. Li, Y.B. Xu, Z.H. Lai, L.T. Shen, Y.L. Bai, "Dynamic recrystalization induced by plastic deformation at high strain rate in a Monel alloy," *Materials Science and Engineering A*, no. 276, pp. 250-256, 2000.